



# Mechanical surface smoothing of micron-sized iron powder for improved silica coating performance as soft magnetic composites

Peter Slovenský<sup>a,b,\*</sup>, Peter Kollár<sup>a</sup>, Nanxuan Mei<sup>b</sup>, Miloš Jakubčín<sup>a</sup>, Adriana Zeleňáková<sup>a</sup>, Maroš Halama<sup>c</sup>, Inger Odnevall Wallinder<sup>b</sup>, Yolanda S. Hedberg<sup>b,\*</sup>

<sup>a</sup> Institute of Physics, Faculty of Science, Pavol Jozef Šafárik University, Park Angelinum 9, 04154 Košice, Slovakia

<sup>b</sup> KTH Royal Institute of Technology, School of Engineering Sciences in Chemistry, Biotechnology and Health, Department of Chemistry, Division of Surface and Corrosion Science, Drottning Kristinas väg 51, SE-10044 Stockholm, Sweden

<sup>c</sup> Technical University of Kosice, Faculty of Materials, Metallurgy and Recycling, Institute of Materials, Letná 9, 042 00 Košice, Slovakia

## ARTICLE INFO

### Keywords:

Soft magnetic composite  
Cyclic voltammetry  
XPS  
TEOS  
SiO<sub>2</sub>  
Coating

## ABSTRACT

Producing defect-free and durable coatings that can withstand elevated annealing temperatures is important when preparing soft magnetic composites. A mechanical surface smoothing method was employed on water atomized Fe powder as an alternative to surfactants, before applying a SiO<sub>2</sub> coating via the surfactant-free Stöber method. This study evaluated the effect of mechanical surface smoothing and the number of SiO<sub>2</sub> coating layers on iron powders of different magnetic properties compared with non-coated iron powders. Electrochemical, microscopic, spectroscopic, and electro-magnetic methods were used to characterize the coating- and the magnetic properties. Sulphur and manganese were present in the outermost (5–10 nm) surface oxide of the non-smoothed angular iron powders, whereas absent in the case of the smoothed, more spherical particles. The surface coverage of the SiO<sub>2</sub> coatings and the magnetic properties were significantly improved for the surface-smoothed iron powders compared to the non-smoothed reference powders. The lack of electrochemical signal from iron oxides of the SiO<sub>2</sub>-coated smoothed particles indicated close-to-complete surface coverage of the coating, also confirmed by electron microscopy. Signals from SiO<sub>2</sub> and organic residues of the coating procedure increased with the number of coating procedures. The compacted surface smoothed Fe/SiO<sub>2</sub> powder showed substantially reduced total energy losses compared to compacted non-smoothed reference powders.

## 1. Introduction

Iron (Fe) powder particles are commonly coated to improve their corrosion resistance [2–4], increase their electrical resistivity [5,6] or to enhance their microwave absorbing properties [7]. The quality of the coatings depends on their homogeneity and adhesion to the particle surfaces. Surfactants are usually used in coating strategies in order to facilitate their adhesion [8,9]. Surfactants have also been shown to possess corrosion inhibiting properties when added to the acid cleaning solution prior to coating procedures [10].

Producing defect-free and durable coatings is also important when preparing soft magnetic composites (SMC's). These materials are characterized as ferromagnetic powder particles (core) covered by a homogenous non-conductive insulating layer (shell). Subsequently, these powder particles are compacted into the desired shape followed by annealing. Annealing is essential to remove accumulated

dislocations and lattice distortions that worsen the magnetic properties of the final product. The main advantages of SMC's, as compared to laminated steel cores, are their high electrical resistance which result in low energy losses while still maintaining relatively high permeability and low coercivity [11]. SMC's are suitable for various alternating current and direct current applications as core materials for e.g. electric motors, transformers or sensors even at medium and high frequencies [12]. If further processed, the coatings need to endure high pressures upon compaction as well as high temperatures [13].

In general, insulating coatings can be inorganic [14–16], organic [17–19] or mixed (organics doped with inorganic compounds) [20,21]. Since organic coatings are not suitable for higher temperatures, SMCs with organic coatings are annealed only at low temperatures (up to 400 °C) [22]. SiO<sub>2</sub> (silica) is a coating suitable for elevated annealing temperatures, conditions that are efficient to remove dislocations and defects. It has previously been shown that silica shells are unlikely to

\* Corresponding authors at: Institute of Physics, Faculty of Science, Pavol Jozef Šafárik University, Park Angelinum 9, 04154 Košice, Slovakia (P. Slovenský). KTH Royal Institute of Technology, Dept. Chemistry, Div. Surface and Corrosion Science, Drottning Kristinas väg 51, 10044 Stockholm, Sweden (Y.S. Hedberg).

E-mail addresses: [peter.slovensky@gmail.com](mailto:peter.slovensky@gmail.com) (P. Slovenský), [yolanda@kth.se](mailto:yolanda@kth.se) (Y.S. Hedberg).

<https://doi.org/10.1016/j.apsusc.2020.147340>

Received 16 April 2020; Received in revised form 2 July 2020; Accepted 22 July 2020

Available online 28 July 2020

0169-4332/© 2020 The Authors. Published by Elsevier B.V. This is an open access article under the CC BY license

(<http://creativecommons.org/licenses/by/4.0/>).

form homogeneous layers during the unmodified Stöber method [23]. 3-aminopropyltriethoxysilane (APTES) surfactants [24,25] or oleic acid [26] have therefore in previous studies been added to the solution as surface-active agents. Except for the benefit of using surfactants, it is known that an increased surface roughness improves the coating adhesion [27].

The aim of this study was to create a coating durable at elevated temperatures ( $> 400$  °C). We replaced the use of surfactants with a surface smoothing methodology in order to limit the use of chemicals. The SiO<sub>2</sub> coating was applied onto the Fe powders using the unmodified Stöber method [28]. To the best of our knowledge, the effects of surface smoothing of the Fe, or any other, powder particles on the quality of the coating layer have not yet been investigated. However, the effect of this smoothing technique on magnetic properties of a NiFeMo alloy was investigated recently [1]. The aim of this work was further to implement and to validate a novel approach to improve the adhesion of the silica coating on micron-sized Fe powder particles without using any surface-active agents.

## 2. Experimental

### 2.1. Preparation of surface-smoothed Fe powder particles

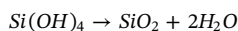
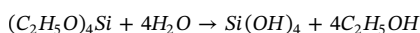
The water-atomised Fe powders (ABC 100.30, Höganäs AB, Sweden) were sieved to particle sizes between 160 µm and 212 µm prior to surface smoothing. This process is described elsewhere [1]. In short, the treatment process was performed in a 1000 mL vial (Ø 100 mm) of a planetary ball mill Retsch PM100 (Haan, Germany) without milling balls, in which SiC abrasive papers (mean grit diameter of 10 µm, Carborundum electrite, Check Republic) were glued (Chemoprén, Pattex, Czech republic) on the inner side and the inner bottom of the cylindrically shaped vial. The smoothening process was conducted for 4.5 h with an angular velocity of 450 rpm. Every 1 min, the direction of the rotation was reversed.

After the smoothing procedure, the powder was separated by a permanent magnet in air and sieved to remove residues from the abrasive papers. The smoothed Fe powder was then repeatedly rinsed and cleaned (at least 5 times) with acetone.

### 2.2. Preparation of SiO<sub>2</sub>@Fe composite powders by the Stöber method

5 g of Fe particles (smoothed or non-smoothed for comparison) were dispersed in 160 mL isopropyl alcohol (Sigma-Aldrich, 99%) by mechanical stirring (Heidolph, Schwabach, Germany, 280 rpm, propeller-shaped stainless steel anchor, with active diameter of 50 mm) for 10 min at room temperature, followed by the addition of 16 mL tetraethyl orthosilicate TEOS (Sigma-Aldrich, 98%) and 4 mL aqueous ammonia (Sigma-Aldrich, 25%). The mixture was then stirred for another 7 h in a cylindrical vessel (Ø 90 mm). Finally, the coated powder was rinsed with isopropyl alcohol three times and dried at room temperature.

The process of silicon dioxide formation from TEOS is described by the following equations, [26]:



These equations were repeated once (in the following denoted 1 layer) and twice (2 layers). In total, the following samples were prepared and investigated:

- Sample 1 (nsm): non-smoothed Fe (for comparison)
- Sample 2 (sm): smoothed Fe (for comparison)
- Sample 3 (nsm-1. l): non-smoothed Fe with one layer of SiO<sub>2</sub> (for comparison)
- Sample 4 (sm-1. l): smoothed Fe with one layer of SiO<sub>2</sub>

- Sample 5 (sm-2. l): smoothed Fe with two layers of SiO<sub>2</sub>

### 2.3. Preparation of compacted samples

4 g of smoothed or non-smoothed powders were mounted in a pressing form with a sprayed lubricant layer (Loctite 8191, Henkel, Düsseldorf, Germany). Pressing was carried out with a holding time of 5 min at a temperature of 400 °C and pressure of 700 MPa in an argon atmosphere. The pressed sample was left in the press until it was cooled to room temperature. After pressing, a ring-shaped sample with an inner diameter of 18 mm and an outer diameter of 24 mm was obtained. The height of the ring was  $2.5 \pm 0.1$  mm.

### 2.4. X-ray photoelectron spectroscopy (XPS)

The outermost surface (5–10 nm) composition was investigated by means of X-ray photoelectron spectroscopy (XPS) using a Kratos Analytical UltraDLD spectrometer (monochromatic 150 W Al X-ray source on areas sized  $700 \times 300$  µm<sup>2</sup>). Duplicate measurements were performed for each powder. Wide spectra and high-resolution spectra (20 eV pass energy) were acquired for Si 2p, Mn 2p, Fe 2p, S 2p, N 1s, O 1s, using C1s as energy reference (285.0 eV).

### 2.5. IR spectroscopy

A LUMOS FT-IR microscope (ATR mode, liquid nitrogen cooled mercury cadmium telluride detector, resolution  $4.0$  cm<sup>-1</sup>) was used to analyze the different powders. A background spectrum on gold was obtained directly before the measurements and used as background spectrum. Each spectrum was based on 512 scans both for the samples and the background. The ATR crystal pressure setting was selected as low. At least two different measurements of each powder (different batches of the powders) were conducted and averaged for each powder type.

### 2.6. Scanning electron microscopy

Scanning electron microscopy (FEI XL30 SEM, 20 kV, < 8,000 times magnification, secondary electron imaging) was used for investigation of the powder morphology. The powders were fixed on carbon tape. For cross-section analysis, the powders were embedded in conductive bakelite resin, grounded, and polished to 3 µm with diamond paste (DP-stick P, Struers, Denmark).

### 2.7. Cyclic voltammetry

Cyclic voltammetry was carried out on all powders (both coated and uncoated for comparison). The buffer was prepared by mixing 100 mL of 0.05 M disodium hydrogen orthophosphate (Na<sub>2</sub>HPO<sub>4</sub>, analytical grade) with 22 mL of 0.1 M sodium hydroxide (NaOH) to obtain a pH of 11.6. This pH is high enough to enable solid–solid transition peaks for Fe oxides, but sufficiently low to avoid rapid dissolution of the SiO<sub>2</sub> layer. The powders were immobilized on the tip of a paraffin-impregnated graphite electrode (PIGE) acting as the working electrode. The counter electrode (platinum wire) and the reference electrode (Ag/AgCl saturated KCl) were placed in the electrolyte with approx. 1 cm spacing between them. The open-circuit potential (OCP) was initially determined as the starting point for cyclic voltammetry measurements. The potential was then swept towards more negative potential values to approximately  $-1.4$  V (vs. Ag/AgCl), after which the potential was swept anodically to more positive potential values to  $+ 0.2$  V at a scan rate of 0.5 mV/s.

## 2.8. Electro-magnetic measurements and density evaluation on compacted samples

Specific electrical resistivity measurements on compacted samples were conducted by a standard four-point method. Voltage measurements were performed ten times at constant current (0.2 A) on different positions on the sample from which the average voltage was determined. The deviation of the measurements was  $\pm 0.1$  mV for samples 1, 2 and 3, and  $\pm 1$  mV for samples 4 and 5. Complex permeability measurements were conducted by an impedance analyser (HP4194A) at a frequency of 100 Hz. The coercivity (A/m) was measured using a Foerster Koerzimat 1.097 HCJ instrument. Total energy losses ( $J/m^3$ ) were measured using a DC fluxmeter-based hysteresisgraph for very low frequencies (in the frequency range of 1 Hz to 100 Hz), using a DC-AC permeameter AMH-1 K-S (in the frequency range of 100 Hz to 800 Hz), and a MATS-2010SA—AC Hysteresisgraph (in the frequency range of 1000 Hz to 30000 Hz) at the maximum magnetic induction  $B_{max}$  of 0.2 T. The non-smoothed samples were only measurable up to a frequency of 10 kHz. The calculated density of the compacted samples was determined as the mass to sample volume fraction. The dimensions of the sample were averaged based on 10 separate measurements.

## 3. Results and discussion

### 3.1. Surface morphology, SEM examinations

SEM images of the uncoated Fe powders before and after the smoothing process are presented in Fig. 1. The particle size for both non-smoothed and smoothed particles ranged from 160 to 212  $\mu m$ . After the smoothing process, sieving was needed mainly due to the presence of small fragments that were ripped off during the mechanical

treatment of the powders. The smoothed powder particles were characterized by surfaces without any sharp edges or protrusions and by a more spherical shape because the protruding parts were rolled inside during the process as is depicted in Fig. 1.

SEM images of smoothed Fe particles with two layers of  $SiO_2$  (sm-2.1) are presented in Fig. 2. The surface of the Fe particles was entirely coated with spherical  $SiO_2$  particles without any visible gaps in the coating. In the cross-section view of the coated Fe samples, the coating layer thickness was not possible to accurately determine by means of SEM and was mostly below 1  $\mu m$  (data not shown).

### 3.2. Surface characterization

Cyclic voltammetry was used to investigate any Fe oxidation peaks that would indicate a disrupted  $SiO_2$  coating on the Fe powders. The dashed lines mark the positions of the two Fe oxidation peaks, Fig. 3. The non-smoothed and the non-coated reference powder showed peaks at  $-1$  V (A1) and  $-0.76$  V (A2). These potentials were slightly shifted compared to literature findings ( $-1.15$  (A1) and  $0.95$  V (A2) at pH 13) [29] due to a lower solution pH (11.6). Fe oxidation peaks were also present, but less evident for the non-smoothed and the 1-layer coated reference powder, Fig. 3, indicative of a non-complete coating coverage. None of the smoothed and coated (1 or 2 layers) powders showed any Fe oxidation peaks, which indicates a relatively good surface coverage with negligible exposure of Fe surfaces to the solution. It is further notable that the hydrogen evolution peak (the rapid increase of the negative current at about  $-1.2$  to  $-1.4$  V) shifted in the case of the coated powders, Fig. 3. This is probably related to higher catalytic activities of Fe metal as compared to  $SiO_2$  [30]. The hydrogen evolution peak was the most positive peak for the non-smoothed non-coated reference powder, followed by the non-smoothed 1-layer coated reference powder, while there seems to be no difference in the 1- or 2-layer

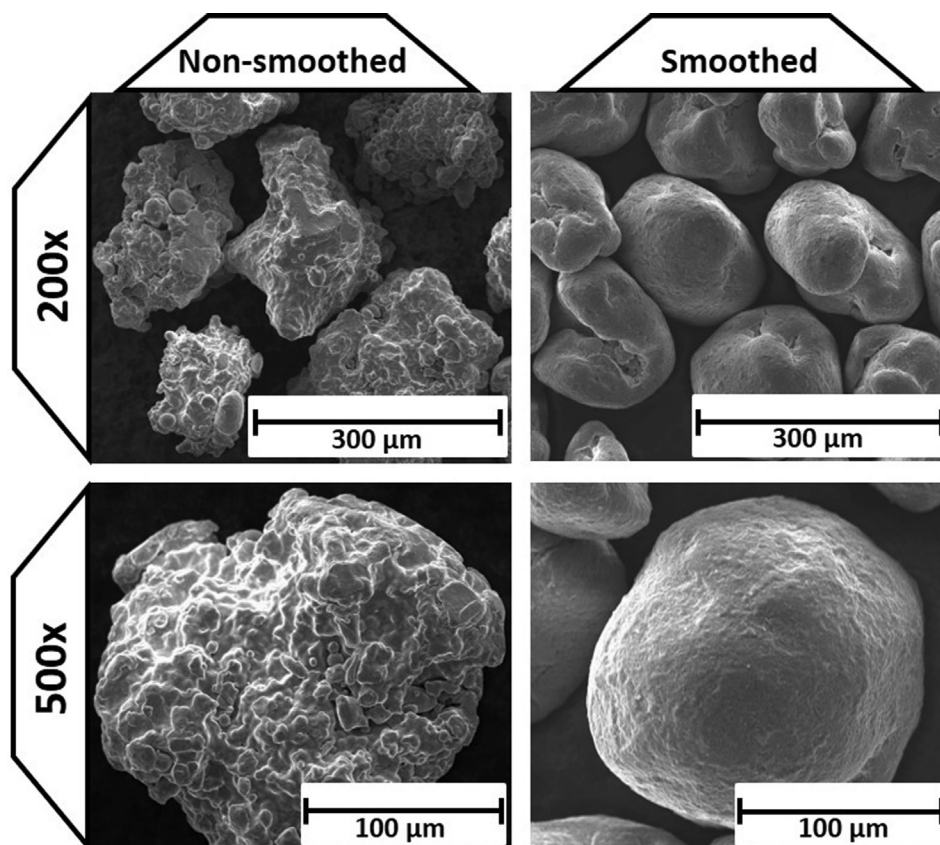


Fig. 1. SEM images (secondary electrons) of the smoothed and the non-smoothed Fe powder at different magnifications.

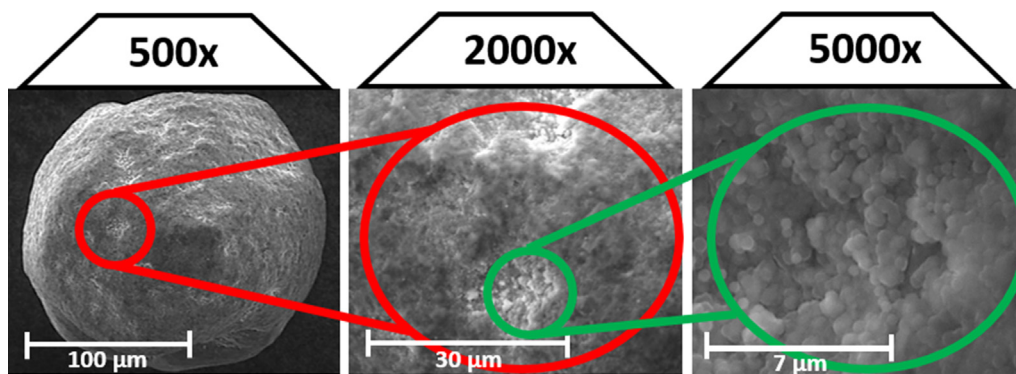


Fig. 2. SEM images at different magnifications showing the smoothed and coated Fe powder (sm-2. 1) and the SiO<sub>2</sub> coating at different magnifications (increasing from left to right).

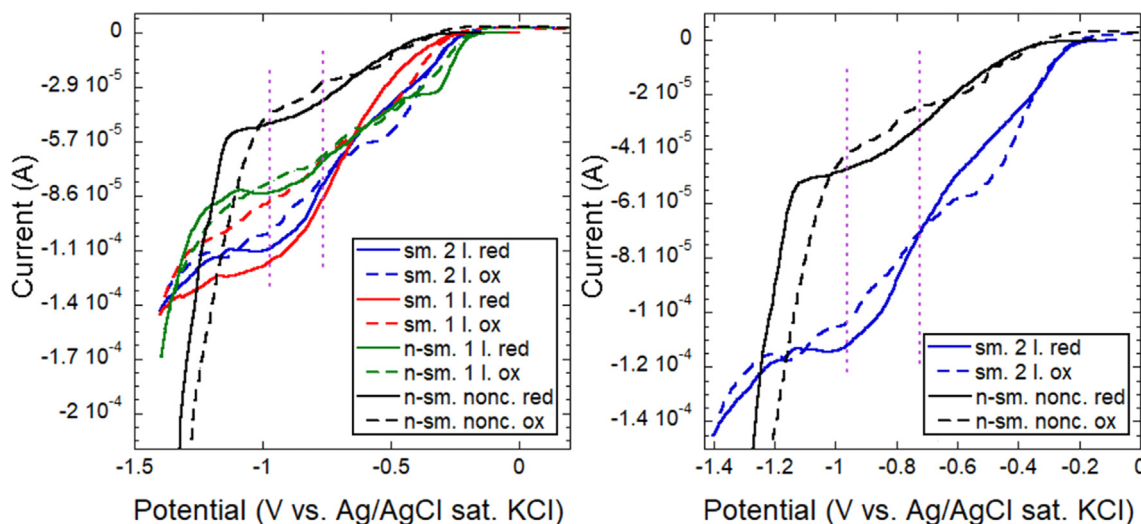


Fig. 3. Cyclic voltammograms at pH 11.6 from the scan started at the OCP potential and continued cathodically (solid lines) to  $-1.4$  V followed by oxidation (anodic scan, dashed line) to  $0.2$  V (vs. Ag/AgCl sat. KCl.  $0.5$  mV/s). The dotted vertical lines (purple) indicate the Fe oxide peak positions. The right graph shows a magnification of the non-smoothed non-coated Fe powder and the smoothed 2-layer coated Fe powder. sm. – smoothed; n-sm. – non-smoothed; l. – layer; nonc. – non-coated; red. – reduction; ox. – oxidation.

coated smoothed Fe powders having the most negative hydrogen evolution peak, Fig. 3. All coated Fe powders revealed reduction peaks at about  $-0.83$  and  $-0.95$  V with corresponding oxidation peaks at  $-0.85$  and  $-0.6$  V. Since SiO<sub>2</sub> is electro-inactive [31], these peaks are suggested to derive from organic species generated during the TEOS-synthesis procedures.

Compositional measurements of the outermost surface by means of XPS (Table 1) clearly revealed an influence of the smoothing process

of the surface composition of the Fe powder. Manganese and sulphur were observed on the non-smoothed Fe powders, whereas absent on the smoothed Fe powders. This observation is in good agreement with previous findings [32], in which these elements were almost completely removed from the surface of water-atomized Fe powders after surface etching. The binding energies (Table 1) of XPS imply sulphur to be present as sulfate [33] and manganese in an oxidized form (di-, tri- and/or tetravalent) [34]. Fe was observed for both the non-smoothed

Table 1

Binding energies of detailed spectra and wide spectra (when charging effects were observed in the detailed spectra), and the atomic mass ratio of silicon compared with silicon and oxygen. n-sm – non-smoothed; sm – smoothed; 1.l – 1 layer; 2.l – 2 layers; SiO<sub>2</sub>@Fe – SiO<sub>2</sub>-coated Fe powders; < LOD – below limit of detection.

Element/eV <sup>a</sup>	Sample 1 n-sm Fe	Sample 2 sm Fe	Sample 3 n-sm SiO <sub>2</sub> @Fe 1.l	Sample 4 sm SiO <sub>2</sub> @Fe 1.l	Sample 5 sm SiO <sub>2</sub> @Fe 2.l
Fe 2p <sub>3/2</sub>	711.0 ± 0.1 712.4 ± 0.9	710.8 ± 0.1 713.6 ± 0.2	< LOD	< LOD	< LOD
Si 2p (wide spectra)	< LOD	< LOD	103.0	103.0	103.0
Si 2p (detailed spectra)	< LOD	< LOD	Charging effects + ≈ 2 eV	Charging effects + ≈ 4 eV	Charging effects + ≈ 9 eV
O 1s (wide spectra)	530.0	531.0	532.0	532.0	532.0
O 1s (detailed spectra)	530.1 ± 0.1 531.8 ± 0.0	530.0 ± 0.1 532.0 ± 0.1	Charging effects + ≈ 2 eV	Charging effects + ≈ 4 eV	Charging effects + ≈ 9 eV
	534.0 ± 0.4	533.7 ± 0.1	< LOD	< LOD	< LOD
Mn 2p <sub>3/2</sub>	641.4 ± 0.1 643.5 ± 0.2	< LOD	< LOD	< LOD	< LOD
S 2p <sub>3/2</sub>	169.2 ± 0.4	< LOD	< LOD	< LOD	< LOD
Si/(Si + O) at%	< LOD	< LOD	28.9	24.2	35.9

<sup>a</sup>Binding energy reference C 1s at 285.0 eV.

and smoothed Fe powders only in its oxidized form (probably trivalent Fe oxide [34]). The corresponding oxygen peak at 530 eV can at least partially be assigned to oxygen bound to Fe [35]. Nitrogen (at 400 eV) was observed for the smoothed Fe powder. Carbon was detected for all samples, mainly corresponding to adventitious carbon [36].

XPS measurements of the coated samples revealed only peaks for silicon, oxygen and carbon. The silicon and oxygen peaks originate from the TEOS treatment [37] and carbon both from adventitious carbon as well as from contamination during preparation and/or the acetone rinsing procedure. The absence of any Fe signal indicates that the SiO<sub>2</sub> coating was fully covering the Fe particles with a thickness of at least 5 nm (the information depth of XPS is 5–10 nm). The measurements showed shifted peak positions of Si 2p and O 1s to higher binding energies in the detailed spectra due to charging effects that became more evident with time and that were not possible to compensate for using the charge neutralizing system. These shifts in binding energies increased for the smoothed as compared to the non-smoothed coated Fe powders and with the number of SiO<sub>2</sub> layers. Similar findings have been reported in the literature [55]. Charge compensation was possible for the wide spectra due to rapid data acquisition. The compositional evaluation of the outermost surface of the SiO<sub>2</sub>-coated particles was hence evaluated from the wide spectra, see Table 1. The observed silicon to oxygen atomic ratio ranged from 24 to 36%, Table 1, i.e. within the range of stoichiometric SiO<sub>2</sub> (33%). The difference is mainly explained by oxygen bound to adventitious carbon.

The IR spectra of the coated and uncoated Fe particles are presented in Fig. 4. The overall spectra show the presence of both organic and inorganic components within the SiO<sub>2</sub> layer(s). Peaks were observed at

2360 cm<sup>-1</sup> and 2340 cm<sup>-1</sup> corresponding gaseous to CO<sub>2</sub> [38,39] and noise peaks in the ranges of 4000 cm<sup>-1</sup> to 3450 cm<sup>-1</sup> and 2050 cm<sup>-1</sup> to 1250 cm<sup>-1</sup>, which correspond to water vapor [40]. The visible water and CO<sub>2</sub> peaks were probably caused by the fact that gold, which was used for background subtraction, reflects more infrared light than the Fe powders. The small, distinct, peak at 670 cm<sup>-1</sup> (gaseous CO<sub>2</sub> peak [38,39]), visible for all samples, originates from the background subtraction aiming to remove water vapor.

The non-smoothed water atomized Fe powder (sample 1- nsm) showed typical iron oxide peaks, most probably assigned to Fe<sub>2</sub>O<sub>3</sub>, Fe<sub>3</sub>O<sub>4</sub>, or FeOOH [41,42]: a broad peak ranging from 3600 cm<sup>-1</sup> to 3000 cm<sup>-1</sup> (stretching vibrations of adsorbed H<sub>2</sub>O molecules), peaks at 1610 cm<sup>-1</sup> (H-O-H bending vibrations), a broad double peak at 1050 and 1100 cm<sup>-1</sup> (possibly related to iron oxyhydroxide bands [42]), and a peak starting around 870 cm<sup>-1</sup>, which is probably indicating the start of the strongest peak of the Fe-O lattice vibration at 540–600 cm<sup>-1</sup> (outside of the measurement window). These peaks were not observed on the smoothed Fe powder (sample 2 - sm), indicative of a very thin (< detection depth of ATR-IR) iron oxide or a different type of iron oxide. Two broad and weak bands at 870 and 670 cm<sup>-1</sup> were observed in the case of the smoothed Fe particles (sample 2). These peaks can be assigned to FeO [43]. It seems hence that the surface smoothing procedure substantially reduced the initial Fe oxides. The spectra of the SiO<sub>2</sub>-coated Fe powder (samples 3–5) were in a good agreement with literature findings [44]. The peak at 945 cm<sup>-1</sup> corresponds to TEOS (rocking vibration of C-H bonds in CH<sub>3</sub>), the peaks at 800 and 1060 cm<sup>-1</sup> to asymmetrical valence vibration (stretching) of SiO<sub>4</sub> and the Si-O-Si group, respectively, and the peaks at 1100 cm<sup>-1</sup> and broad

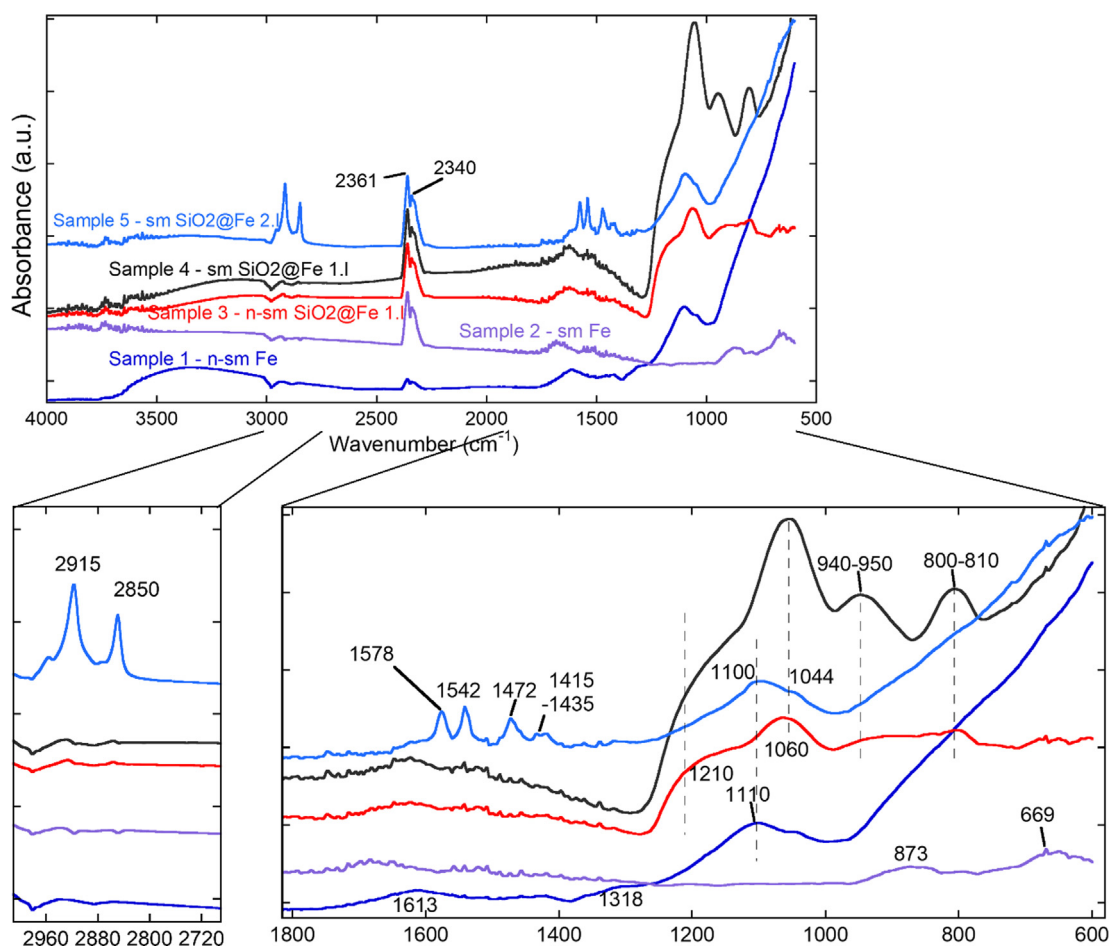


Fig. 4. ATR-FTIR average spectra of all Fe powders; overview spectra (top), magnified areas from 3000 to 2700 cm<sup>-1</sup> and 1800 to 800 cm<sup>-1</sup> (bottom) n-sm – non-smoothed; sm – smoothed; 1.1 – 1 layer; 2.1 – 2 layers; SiO<sub>2</sub>@Fe – SiO<sub>2</sub>-coated Fe powders.

shoulder centred at  $1210\text{ cm}^{-1}$  to C-O and C-H bonds from  $\text{CH}_3$  groups, respectively. These peaks are broad due to overlapping peaks related to the presence of ethanol and ammonia from the coating procedure, as also reported previously [44]. The distinct peaks at  $2850$  and  $2915\text{ cm}^{-1}$  that most probably correspond to the  $\text{CH}_2$  symmetric stretch and  $\text{CH}_2$  asymmetric stretch [45] deriving from organic pollutants, were only visible for the  $\text{SiO}_2$ -coated Fe powder (2 layers, sample 5). Smaller, but distinct peaks visible for sample 5 around  $1415$ – $1435$  (e.g. assigned to  $\text{CH}_3$  umbrella band or  $\text{CH}_3$  deformation band [45]),  $1470$  ( $\text{CH}_2$  scissors band,  $\text{CH}_3$  deformation band [45]),  $\text{CH}_2$  deformation band [46], or carbonate [47]),  $1540$  (OH deformation [48] or carbonate [47]), and  $1580$  (CO stretch [45])  $\text{cm}^{-1}$  might also derive from organic pollutants or combustion products of organic pollutants.

### 3.3. Characterization of magnetic properties

As the produced SMC materials are intended for electro-magnetic applications, it was necessary to perform a basic magnetic test to determine whether the smoothing itself had a negative effect on the magnetic properties or not. Satisfactory characterization of the properties of the SMC materials requires at least the determination of their specific resistivity, coercivity, permeability, and energy losses. Electro-magnetic properties (specific resistivity, coercivity, and maximum values of real part of relative initial permeability) and density for the compacted powders are presented in Table 2.

In this study, the sample density is mainly influenced by the compaction pressure and the increased temperature ( $400\text{ }^\circ\text{C}$ ) during compaction [49]. The highest density achieved ( $7.84\text{ g/cm}^3$ ) was observed for the noncoated, nonsmoothed sample. The shape of this powder is ideal for pressing [50], numerous protrusions fit together and become entangled. After removal of these protrusions, by the smoothing procedure, the density after compression decreased to  $7.49\text{ g/cm}^3$ , Table 2 (sample 2). We speculate that the characteristics of the  $\text{SiO}_2$  coating can be responsible for the increase in the density of compacts of coated powders (samples 4–5) when compared to the non-coated reference (sample 2). As can be seen in Fig. 2, the top layer of the coating is composed of spherical nanoparticles which might partly act as a lubricant.

The specific resistivity of the smoothed and coated samples ranged from  $1.9 \cdot 10^{-7}$  (n-sm  $\text{SiO}_2$ @Fe 1.1) to  $1.0 \cdot 10^{-5}$  (sm  $\text{SiO}_2$ @Fe 2.1). The high conductivity observed even after successful coating can be explained by the coating thickness, being in the nanometer range. We speculate that the thin layer has different electric properties than its corresponding bulk form [51].

The coercivity of a given magnetic material describes whether it can easily be demagnetized (for soft magnetic materials:  $H_c \leq 1000$ ) or more difficult (for hard magnetic materials:  $H_c > 1000$ ). The coercivity can be affected by the magnetic anisotropy and by inner imperfections such as inclusions, plastic deformations, and grain boundaries that depend on the crystal grain size [52]. Compacting at high pressure (in our case  $700\text{ MPa}$ ) generates inner plastic deformations,

**Table 2**

Electro-magnetic properties and density of the Fe-powders. n-sm – non-smoothed; sm – smoothed; 1.1 – 1 layer; 2.1 – 2 layers;  $\text{SiO}_2$ @Fe –  $\text{SiO}_2$ -coated Fe powders.

	Sample 1 n-sm Fe	Sample 2 sm Fe	Sample 3 n-sm $\text{SiO}_2$ @Fe 1.1	Sample 4 sm $\text{SiO}_2$ @Fe 1.1	Sample 5 sm $\text{SiO}_2$ @Fe 2.1
Density [ $\text{g/cm}^3$ ]	$7.84 \pm 0.2$	$7.49 \pm 0.2$	$7.70 \pm 0.2$	$7.60 \pm 0.2$	$7.60 \pm 0.3$
Specific resistivity [ $\Omega\text{-m}$ ]	$1.7 \pm 0.2 \cdot 10^{-7}$	$1.5 \pm 0.08 \cdot 10^{-7}$	$1.9 \pm 0.1 \cdot 10^{-7}$	$3.0 \pm 0.4 \cdot 10^{-6}$	$1.0 \pm 0.4 \cdot 10^{-5}$
Coercivity [A/m]	$380 \pm 0.7$	$430 \pm 2.5$	$390 \pm 0.8$	$500 \pm 1.1$	$480 \pm 0.4$
DC energy loss [ $\text{J/m}^3$ ]	$65 \pm 1.3$	$68 \pm 1.4$	$65 \pm 1.3$	$79 \pm 1.6$	$75 \pm 1.5$
Permeability $\mu_r$ [-]	$105 \pm 1$	$105 \pm 1.2$	$100 \pm 1$	$95 \pm 1.1$	$83 \pm 1$

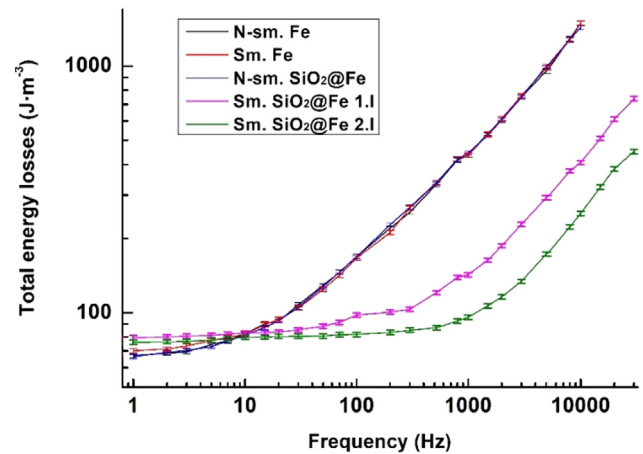


**Fig. 5.** Dependence of total energy losses on the frequency at maximum induction of  $0.2\text{ T}$ . n-sm – non-smoothed; sm – smoothed; 1.1 – 1 layer; 2.1 – 2 layers;  $\text{SiO}_2$ @Fe –  $\text{SiO}_2$ -coated Fe powders.

which hinder the domain wall displacement by the stress field surrounding the dislocations. The measured coercivity values of the compacted samples are shown in Table 2. The smoothing procedure caused an increase in coercivity from  $380\text{ A/m}$  (n-sm Fe) to  $430\text{ A/m}$  (sm Fe), which is due to additional creation of dislocations at the surface during the smoothing process. A further increase of the coercivity for coated samples may be explained by the introduction of further surface defects during the chemical coating process. The negative effect of dislocations on the coercivity, whether generated during pressing or during smoothing, could be relieved by heat treatment.

The specific resistivity values of all investigated samples are important for their total energy losses with frequency. The total energy losses  $W_t$  ( $\text{J/m}^3$ ) can be divided into three parts: hysteresis losses, eddy current losses, and excess losses (or residual losses) [53]. The predominating component that determines the total energy losses observed for the powders of this study is the eddy current loss. Due to the protective  $\text{SiO}_2$  coating on samples 4–5 (sm  $\text{SiO}_2$ @Fe 1.1 and 2.1), the generated eddy current cannot flow through the entire sample but is rather locked inside every powder particle [54]. As a result, lower energy losses were observed for the smoothed and the coated samples (samples 4–5) compared to the non-coated (samples 1–2) and the non-smoothed  $\text{SiO}_2$ @Fe 1.1 (sample 3) samples. The dependence of total energy losses on frequency is presented in Fig. 5.

The results show further a decreasing tendency of the relative initial permeability with improved surface coating characteristics, Table 2. The evolution of complex relative initial permeability of the compacts as a function of frequency is shown in Fig. 6. The samples 1–3 showed a similar trend of the permeability versus frequency. The maximal value of the real part of the complex permeability,  $\mu_r$ , was higher than for coated and smoothed samples (samples 4 and 5), but the  $\mu_r$  of samples

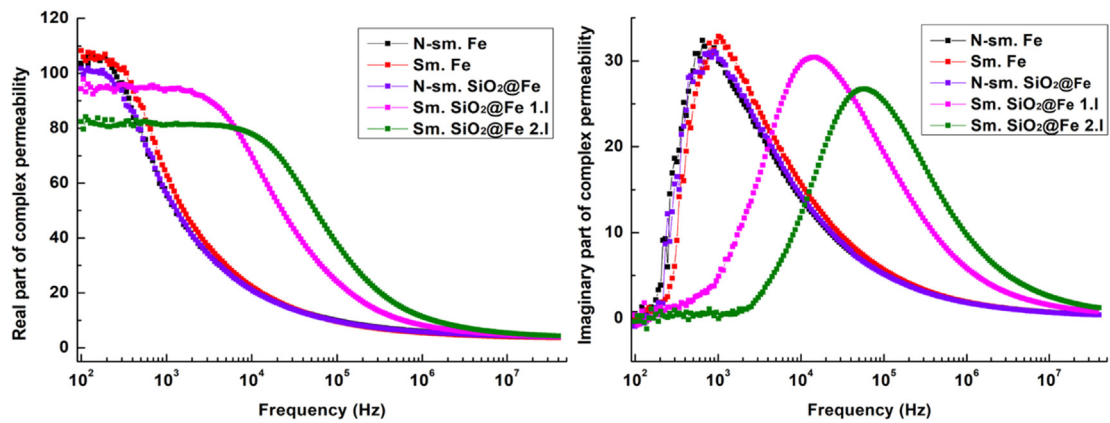


Fig. 6. Real and imaginary parts of complex permeability (unitless) of compacted powders, n-sm – non-smoothed; sm – smoothed; 1.1 – 1 layer; 2.1 – 2 layers; SiO<sub>2</sub>@Fe – SiO<sub>2</sub>-coated Fe powders.

1–3 was only higher in the low frequency ranges. This is due to the non-present (samples 1–2) or bad insulation (sample 3) between powder particles. The compacts fabricated from the smoothed and coated powders (samples 4 and 5) exhibit stable values of  $\mu_r$  with a significant decrease at higher frequencies (4 kHz and 20 kHz, respectively) and are hence more suitable for higher frequency applications. The imaginary part of the complex relative permeability confirms the improved magnetic properties of samples 4 and 5, as the peaks are moved to higher frequencies, Fig. 6.

For the highest possible permeability, the extent of insulation should generally be minimized. When the coating layer thickens, the relative initial permeability hence slightly decreases [54].

Overall, the smoothing process introduced some additional plastic deformations, which led to slightly increased coercivity but improved the coating quality. This resulted in an increase in resistance and a reduction in energy losses of up to 75% at 10 kHz compared to SMC's made of non-coated or non-smoothed coated Fe powder.

#### 4. Conclusions

1. The mechanical surface smoothing substantially changed the shape of the water-atomized Fe powders towards more spherical particles, changed the chemical surface composition [removal of manganese and sulphur from the outermost (5–10 nm) surface], and reduced the surface iron oxide thickness at the surface.
2. Surface smoothing slightly lowered the compressibility of the powders and raised the coercivity that resulted from the additional mechanical stresses applied on the surface during the process. Neither the specific resistivity nor the maximum values of the real part of the relative initial permeability were affected by the smoothing process.
3. Cyclic voltammetry indicated a non-complete surface coverage of the coating for the coated non-smoothed powders, but an almost complete coverage for the smoothed and the coated (1 or 2 layers) powders, as judged from the absence of peaks related to iron oxidation. XPS confirmed complete coverage and SiO<sub>2</sub> to be the main component of the layers. The layer thickness remained in the nanometer-range (< 1  $\mu\text{m}$ ), as judged from cross-section SEM images.
4. Organic residues were observed within the TEOS-formed SiO<sub>2</sub> coating by means of cyclic voltammetry, XPS, and ATR-IR spectroscopy measurements.
5. SMC's made of surface-smoothed and coated Fe powder revealed significantly (75%) lower total energy losses at higher frequencies compared to SMC's made of non-coated or non-smoothed coated Fe powder.
6. Overall, this study indicates that surface smoothing of water atomized Fe powder particles is a way forward to improve the SiO<sub>2</sub>

coating characteristics. Smoothed Fe/SiO<sub>2</sub> SMC's could hence be produced for applications in medium frequencies without using any surfactants during the coating process.

#### CRediT authorship contribution statement

**Peter Slovenský:** Conceptualization, Validation, Methodology, Investigation, Writing - original draft, Visualization, Project administration, Funding acquisition. **Peter Kollár:** Conceptualization, Methodology, Supervision, Writing - review & editing. **Nanxuan Mei:** Investigation. **Miloš Jakubčín:** Investigation. **Adriana Zeleňáková:** Resources. **Maroš Halama:** Resources. **Inger Odnevall Wallinder:** Investigation, Writing - review & editing. **Yolanda S. Hedberg:** Conceptualization, Methodology, Validation, Resources, Writing - review & editing, Visualization, Supervision, Project administration, Funding acquisition.

#### Declaration of Competing Interest

The authors declare that they have no known competing financial interests or personal relationships that could have appeared to influence the work reported in this paper.

#### Acknowledgements

Experimental and supervision assistance by Dr. Gunilla Herting and Dr. Jonas Hedberg, KTH Royal Institute of Technology, Stockholm, Sweden are highly acknowledged.

Funding: This work was supported by the Slovak Research and Development Agency [grant no. APVV-15-0115]; the Scientific Grant Agency of the Ministry of Education, Science, Research and Sport of the Slovak Republic and the Slovak Academy of Sciences [grant no. VEGA 1/0143/20]; the Swedish Research Council [grant no. 2019-03657]; the Swedish Foundation for Strategic Research [grant no. FFL18-0173] and KTH faculty grants.

#### References

- [1] P. Kollár, P. Slovenský, D. Olekšáková, M. Jakubčín, Z. Birčáková, J. Füzér, R. Bureš, M. Fáberová, Preparation and magnetic properties of NiFeMo powdered compacts of powder elements with smoothed surfaces, *J. Magn. Mater.* 494 (2020) 1–12, <https://doi.org/10.1016/j.jmmm.2019.165770>.
- [2] S. Rebeyrat, J.L. Grosseau-Poussard, J.F. Dinhut, P.O. Renault, Oxidation of phosphated iron powders, *Thin Solid Films* 379 (1–2) (2000) 139–146, [https://doi.org/10.1016/S0040-6090\(00\)01416-4](https://doi.org/10.1016/S0040-6090(00)01416-4).
- [3] Y. Zhang, A. Bu, Y. Xiang, Y. Yang, W. Chen, H. Cheng, L. Wang, Improving corrosion resistance of carbonyl iron powders by plasma electrolytic deposition, *Mater. Des.* 188 (2020) 180480, <https://doi.org/10.1016/j.matdes.2020.108480>.
- [4] S.S. Maklakov, A.N. Lagarkov, S.A. Maklakov, Y.A. Adamovich, D.A. Petrov, K.N. Rozanov, I.A. Ryzhikov, A.Y. Zarubina, K.V. Pokholok, D.S. Filimonov,

- Corrosion-resistive magnetic powder Fe@SiO<sub>2</sub> for microwave applications, *J. Alloys Compd.* 706 (2017) 267–273, <https://doi.org/10.1016/j.jallcom.2017.02.250>.
- [5] B. Meng, J. Hou, F. Ning, B. Yang, B. Zhou, R. Yu, Low-loss and high-induction Fe-based soft magnetic composites coated with magnetic insulating layers, *J. Magn. Mater.* 492 (2019) 165651, <https://doi.org/10.1016/j.jmmm.2019.165651>.
- [6] H.-I. Hsiang, L.-F. Fan, J.-J. Hung, Effects of the sodium stearate addition on the corrosion resistance and electromagnetic properties of phosphatized iron-based SMCs, *J. Magn. Mater.* 490 (2019) 165532, <https://doi.org/10.1016/j.jmmm.2019.165532>.
- [7] Y. Zhou, H. Xie, W. Zhou, Z. Ren, Enhanced antioxidation and microwave absorbing properties of SiO<sub>2</sub>-coated flaky carbonyl iron particles, *J. Magn. Mater.* 446 (2018) 143–149, <https://doi.org/10.1016/j.jmmm.2017.09.022>.
- [8] C.h. Guo, Y. Zuo, X. Zhao, J. Xiong, Effects of surfactants on electrodeposition of nickel-carbon nanotubes composite coatings, *Surf. Coat. Technol.* 202 (2008) 3385–3390, <https://doi.org/10.1016/j.surfcoat.2007.12.005>.
- [9] D. Ning, A. Zhang, M. Murtaza, H. Wu, Effect of surfactants on the electrodeposition of Cu-TiO<sub>2</sub> composite coatings prepared by jet electrodeposition, *J. Alloys Compd.* 777 (2019) 1245–1250, <https://doi.org/10.1016/j.jallcom.2018.11.077>.
- [10] M. Motamedi, A.R. Tehrani-Bagha, M. Mahdavian, The effect of cationic surfactants in acid cleaning solutions on protective performance and adhesion strength of the subsequent polyurethane coating, *Prog. Org. Coat.* 77 (2014) 712–718, <https://doi.org/10.1016/j.porgcoat.2013.12.009>.
- [11] K.J. Sunday, M.L. Taheri, Soft magnetic composites: recent advancements in the technology, *Met. Powder Rep.* 72 (2017) 425–429, <https://doi.org/10.1016/j.mprp.2016.08.003>.
- [12] E.A. Périgo, B. Weidenfeller, P. Kollár, J. Füzér, Past, present, and future of soft magnetic composites, *Appl. Phys. Rev.* 5 (2018), <https://doi.org/10.1063/1.5027045>.
- [13] W. Ding, L. Jiang, Y. Liao, J. Song, B. Li, G. Wu, Effect of iron particle size and volume fraction on the magnetic properties of Fe/silicate glass soft magnetic composites, *J. Magn. Mater.* 378 (2018) 232–238, <https://doi.org/10.1016/j.jmmm.2014.09.019>.
- [14] M. Yaghtin, A.H. Taghvaei, B. Hashemi, K. Janghorban, Effect of heat treatment on magnetic properties of iron-based soft magnetic composites with Al<sub>2</sub>O<sub>3</sub> insulation coating produced by sol-gel method, *J. Alloys Compd.* 581 (2013) 293–297, <https://doi.org/10.1016/j.jallcom.2013.07.008>.
- [15] Z. Zhong, Q. Wang, L. Tao, L. Jin, X. Tang, F. Bai, H. Zhang, Permeability dispersion and magnetic loss of Fe/Ni<sub>1-x</sub>Zn<sub>1-x</sub>Fe<sub>2</sub>O<sub>4</sub> soft magnetic composites, *IEEE Trans. Magn.* 48 (2012) 3622–3625, <https://doi.org/10.1109/TMAG.2012.2202271>.
- [16] Y. Peng, J. Nie, W. Zhang, Ch. Bao, J. Ma, Y. Cao, Preparation of soft magnetic composites for Fe particles coated with (NiZn)Fe<sub>2</sub>O<sub>4</sub> via microwave treatment, *J. Magn. Mater.* 395 (2015) 245–250, <https://doi.org/10.1016/j.jmmm.2015.07.071>.
- [17] M.M. Dias, H.J. Mozetic, J.S. Barboza, R.M. Martins, L. Pelegrini, L. Schaeffer, Influence of resin type and content on electrical and magnetic properties of soft magnetic composites (SMCs), *Powder Technol.* 237 (2013) 213–220, <https://doi.org/10.1016/j.powtec.2013.01.006>.
- [18] A.H. Taghvaei, H. Shokrollahi, K. Janghorban, Structural studies, magnetic properties and loss separation in iron-phenolicsilane soft magnetic composites, *Mater. Des.* 31 (2010) 142–148, <https://doi.org/10.1016/j.matdes.2009.06.044>.
- [19] A.H. Taghvaei, A. Ebrahimi, M. Ghaffari, K. Janghorban, Investigating the magnetic properties of soft magnetic composites based on mechanically alloyed nanocrystalline Fe-5wt% Ni powders, *J. Magn. Mater.* 323 (2011) 150–156, <https://doi.org/10.1016/j.jmmm.2010.08.052>.
- [20] T.A. Laxminarayana, K.M. Subhendu, B.G. Fernandes, N. Venkataramani, Study of AC magnetic properties and core losses of Fe/Fe<sub>3</sub>O<sub>4</sub>-epoxy resin soft magnetic composite, *Phys. Proc.* 75 (2015) 1396–1403, <https://doi.org/10.1016/j.phpro.2015.12.157>.
- [21] J. Füzér, M. Strečková, S. Dobák, L. Ďáková, P. Kollár, M. Fáberová, R. Bureš, Y. Osadchuk, P. Kurek, M. Vojtko, Innovative ferrite nanofibres reinforced soft magnetic composite with enhanced electrical resistivity, *J. Alloys Compd.* 753 (2018) 219–227, <https://doi.org/10.1016/j.jallcom.2018.04.237>.
- [22] I. Hematti, H.R. Hosseini, A. Kianvash, The correlations between processing parameters and magnetic properties of an iron-resin soft magnetic composite, *J. Magn. Mater.* 305 (2006) 147–151, <https://doi.org/10.1016/j.jmmm.2005.12.004>.
- [23] Y.-J. Wong, L. Zhu, W.-S. Teo, Y.-W. Tan, Y. Yang, Ch. Wang, H. Chen, Revisiting the Stober method: inhomogeneity in silica shells, *J. Am. Chem. Soc.* 133 (2011) 11422–11425, <https://doi.org/10.1021/ja203316q>.
- [24] J. Wang, X. Fan, Z. Wu, G. Li, Intergranular insulated Fe/SiO<sub>2</sub> soft magnetic composite for decreased core loss, *Adv. Powder Tech.* 27 (2016) 1189–1194, <https://doi.org/10.1016/j.apt.2016.04.002>.
- [25] J. Wang, X. Fan, Z. Wu, G. Li, Synthesis, microstructure and magnetic properties of Fe<sub>3</sub>Si<sub>0.7</sub>Al<sub>0.3</sub>@SiO<sub>2</sub> core-shell particles and Fe<sub>3</sub>Si/Al<sub>2</sub>O<sub>3</sub> soft magnetic composite core, *J. Solid State Chem.* 231 (2015) 152–158, <https://doi.org/10.1016/j.jssc.2015.08.016>.
- [26] B. Yang, Z. Wu, Z. Zou, R. Yu, High-performance Fe/SiO<sub>2</sub> soft magnetic composites for low-loss and high-power applications, *J. Phys. D: Appl. Phys.* 43 (2010) 1–6, <https://doi.org/10.1088/0022-3727/43/36/365003>.
- [27] R.B. Leggat, S.A. Taylor, S.R. Taylor, Adhesion of epoxy to hydroxylated conversion coatings: II. Surface modification with ionic surfactants, *Colloids and Surfaces A: Physicochem. Eng. Asp.* 210 (2002) 83–94, [https://doi.org/10.1016/S0927-7757\(02\)00210-8](https://doi.org/10.1016/S0927-7757(02)00210-8).
- [28] W. Stöber, A. Fink, E. Bohn, Controlled growth of mono disperse silica spheres in the micron size range, *J. Colloid Interface Sci.* 26 (1968) 62–69, [https://doi.org/10.1016/0021-9797\(68\)90272-5](https://doi.org/10.1016/0021-9797(68)90272-5).
- [29] N. Mei, L. Belleville, Y. Cha, U. Olafsson, I.O. Wallinder, K.-A. Persson, Y. Hedberg, Size-separated particle fractions of stainless steel welding fume particles – A multi-analytical characterization focusing on surface oxide speciation and release of hexavalent chromium, *J. Hazard. Mater.* 342 (2018) 527–535, <https://doi.org/10.1016/j.jhazmat.2017.08.070>.
- [30] H. Alemu, K. Jüttner, Characterization of the electrocatalytic properties of amorphous metals for oxygen and hydrogen evolution by impedance measurements, *Electrochim Acta* 33 (1101–1109) (1988).
- [31] P.A. Nikolaychuk, The revised pourbaix diagram for silicon, *Silicon* 6 (2014) 109–116, <https://doi.org/10.1007/s12633-013-9172-0>.
- [32] J. Wendel, R. Shvab, Y. Cao, E. Hryha, L. Nyborg, Surface analysis of fine water-atomized iron powder and sintered material, *Surf. Interf. Anal.* 50 (2018), <https://doi.org/10.1002/sia.6455>.
- [33] A.L. Neal, S. Techkarnjanaruk, A. Dohnalkova, D. McCready, B.M. Peyton, G.G. Geesey, Iron sulfides and sulfur species produced at hematite surfaces in the presence of sulfate-reducing bacteria, *Geochim Cosmochim Acta* 65 (223–235) (2001), [https://doi.org/10.1016/S0016-7037\(00\)00537-8](https://doi.org/10.1016/S0016-7037(00)00537-8).
- [34] M.C. Biesinger, B.P. Payne, A.P. Grosvenor, L.W.M. Lau, A.R. Gerson, R.S.C. Smart, Resolving surface chemical states in XPS analysis of first row transition metals, oxides and hydroxides: Cr, Mn, Fe, Co and Ni, *Appl. Surf. Sci.* 257 (2717–2730) (2011), <https://doi.org/10.1016/j.apsusc.2010.10.051>.
- [35] J. Benzakour, A. Derja, Characterisation of the passive film on iron in phosphate medium by voltammetry and XPS measurements, *J. Electroanal. Chem.* 437 (1997) 119–124, [https://doi.org/10.1016/S0022-0728\(97\)00337-9](https://doi.org/10.1016/S0022-0728(97)00337-9).
- [36] M.C. Biesinger, X-ray Photoelectron Spectroscopy (XPS) Reference Pages, <http://www.xpsfitting.com/search/label/carbon>, accessed 2020-06-28, (2020).
- [37] Y. Li, Z. Jin, T. Li, Z. Xiu, One-step synthesis and characterization of core-shell Fe@SiO<sub>2</sub> nanocomposite for Cr (VI) reduction, *Sci. Total Environ.* 422 (2012) 260–266, <https://doi.org/10.1016/j.scitotenv.2012.01.010>.
- [38] P.E. Martin, E.F. Barker, The infrared absorption spectrum of carbon dioxide, *Phys. Rev.* 41 (1932) 291–303, [https://doi.org/10.1002/\(SICI\)1096-9918\(199601\)24:1<28::AID-SIA66>3.0.CO;2-G](https://doi.org/10.1002/(SICI)1096-9918(199601)24:1<28::AID-SIA66>3.0.CO;2-G).
- [39] Bio-Rad Laboratories, Inc. SpectraBase; SpectraBase Compound ID = 8A1dEQuRMH SpectraBase Spectrum ID = G4CBuKNSKtQ, [http://spectrabase.com/spectrum/G4CBuKNSKtQ?a=SPECTRUM\\_G4CBuKNSKtQ](http://spectrabase.com/spectrum/G4CBuKNSKtQ?a=SPECTRUM_G4CBuKNSKtQ) (accessed 2020-06-28).
- [40] Bio-Rad Laboratories, Inc. SpectraBase; SpectraBase Compound ID = Cz3wO46i3MG SpectraBase Spectrum ID = BnpceB1yUv, [http://spectrabase.com/spectrum/BnpceB1yUv?a=SPECTRUM\\_BnpceB1yUv](http://spectrabase.com/spectrum/BnpceB1yUv?a=SPECTRUM_BnpceB1yUv) (accessed 2020-06-28).
- [41] M. Ellid, Y. Murayed, M. Zoto, S. Musić, S. Popović, Chemical reduction of hematite with starch, *J. Radioanal. Nucl. Chem.* 258 (2003) 299–305, <https://doi.org/10.1023/A:1026285721065>.
- [42] T.D. Glotch, M.D. Kraft, Thermal transformations of akaganéite and lepidocrocite to hematite: assessment of possible precursors to Martian crystalline hematite, *Phys. Chem. Miner.* 35 (2008) 569–581, <https://doi.org/10.1007/s00269-008-0249-z>.
- [43] L. Zhang, M. Zhou, L. Shao, W. Wang, K. Fan, Q. Qin, Reactions of Fe with H<sub>2</sub>O and FeO with H<sub>2</sub>. A Combined matrix isolation FTIR and theoretical study, *J. Phys. Chem. A* 105 (2001) 6998–7003, <https://doi.org/10.1021/jp010914n> (accessed 2020-06-28).
- [44] B.V. Neamtu, A. Belea, F. Popa, E. Ware, T.F. Marinca, I. Vintiloiu, C. Badaea, M. Pszola, M. Nasui, Properties of soft magnetic composites based on Fe fibres coated with SiO<sub>2</sub> by hydrothermal method, *J. Alloys Compd.* 826 (2020), <https://doi.org/10.1016/j.jallcom.2020.154222>.
- [45] M.E. Jacox, Vibrational and electronic energy levels of polyatomic transient molecules. Supplement B, *J. Phys. Chem. Ref. Data.* 32 (2003) 1–441, <https://doi.org/10.1063/1.1497629>.
- [46] J. Fripiat, M. Pennequin, G. Poncelet, P. Cloos, Influence of the van der Waals force on the infrared spectra of short aliphatic alkylammonium cations held on montmorillonite, *Clay. Miner.* 8 (1969) 119–134, <https://doi.org/10.1180/claymin.1969.008.2.01>.
- [47] M.E. Fleet, Infrared spectra of carbonate apatites: ν<sub>2</sub>-Region bands, *Biomater.* 30 (2009) 1473–1481, <https://doi.org/10.1016/j.biomaterials.2008.12.007>.
- [48] L. Legrand, G. Sagon, S. Lecomte, A. Chausse, R. Messina, A. Raman and infrared study of a new carbonate green rust obtained by electrochemical way, *Corros. Sci.* 43 (2001) 1739–1749, [https://doi.org/10.1016/S0010-938X\(00\)00172-4](https://doi.org/10.1016/S0010-938X(00)00172-4).
- [49] H. Shokrollahi, K. Janghorban, Effect of warm compaction on the magnetic and electrical properties of Fe-based soft magnetic composites, *J. Magn. Mater.* 313 (2007) 182–186, <https://doi.org/10.1016/j.jmmm.2006.12.022>.
- [50] D. Poquillon, J. Lemaître, V. Baco-Carles, Ph. Tailhades, J. Lacaze, Cold compaction of iron powders—relations between powder morphology and mechanical properties. Part I: Powder preparation and compaction, *Powder. Technol.* 126 (2002) 65–74, [https://doi.org/10.1016/S0032-5910\(02\)00034-7](https://doi.org/10.1016/S0032-5910(02)00034-7).
- [51] T.H. DiStefano, M. Shatzkes, Dielectric instability and breakdown in SiO<sub>2</sub> thin films, *J. Vac. Sci. Tech.* 13 (1976) 50, <https://doi.org/10.1116/1.568911>.
- [52] M.F. Campos, A general coercivity model for soft magnetic materials, *Mater. Sci. Forum* 727 (2012) 157–162, <https://doi.org/10.4028/www.scientific.net/MSF.727-728.157>.
- [53] P. Kollár, Z. Birčáková, J. Füzér, R. Bureš, M. Fáberová, Power loss separation in Fe-based composite materials, *J. Magn. Mater.* 327 (2013) 146–150, <https://doi.org/10.1016/j.jmmm.2012.09.055>.
- [54] H. Shokrollahi, K. Janghorban, Soft magnetic materials (SMCs), *J. Mater. Proc. Techn.* 189 (2007) 1–12, <https://doi.org/10.1016/j.jmatproc.2007.02.034>.
- [55] Brian Tielsch, Julia Fulghum, Differential charging in XPS. Part I: demonstration of lateral charging in a bulk insulator using imaging XPS, *Surf. Interf. Anal.* 24 (1) (1996) 28–33, [https://doi.org/10.1002/\(SICI\)1096-9918\(199601\)24:1<28::AID-SIA66>3.0.CO;2-G](https://doi.org/10.1002/(SICI)1096-9918(199601)24:1<28::AID-SIA66>3.0.CO;2-G).